Congenital Brain Abnormalities and Zika Virus: What the Radiologist Can Expect to See Prenatally and Postnatally[1]

Patricia Soares de Oliveira-Szejnfeld, MD
Deborah Levine, MD
Adriana Suely de Oliveira Melo, MD, PhD
Melania Maria Ramos Amorim, MD, PhD
Alba Gean M. Batista, MD
Leila Chimelli, MD, PhD
Amilcar Tanuri, MD, PhD
Renato Santana Aguiar, PhD
Gustavo Malinger, MD, PhD
Renato Ximenes, MD
Richard Robertson, MD
Jacob Szejnfeld, MD, PhD
Fernanda Tovar-Moll, MD, PhD

Purpose: To document the imaging findings associated with congenital Zika virus infection as found in the Instituto de Pesquisa in Campina Grande State Paraiba (IPESQ) in northeastern Brazil, where the congenital infection has been particularly severe.

Materials and Methods: From June 2015 to May 2016, 438 patients were referred to the IPESQ for rash occurring during pregnancy or for suspected fetal central nervous system abnormality. Patients who underwent imaging at IPESQ were included, as well as those with documented Zika virus infection in fluid or tissue (n = 17, confirmed infection cohort) or those with brain findings suspicious for Zika virus infection, with intracranial calcifications (n = 28, presumed infection cohort). Imaging examinations included 12 fetal magnetic resonance (MR) examinations, 42 postnatal brain computed tomographic examinations, and 11 postnatal brain MR examinations. Images were reviewed by four radiologists, with final opinion achieved by means of consensus.

Results: Brain abnormalities seen in confirmed (n = 17) and presumed (n = 28) congenital Zika virus infections were similar, with ventriculomegaly in 16 of 17 (94%) and 27 of 28 (96%) infections, respectively; abnormalities of the corpus callosum in 16 of 17 (94%) and 22 of 28 (78%) infections, respectively; and cortical migrational abnormalities in 16 of 17 (94%) and 28 of 28 (100%) infections, respectively. Although most fetuses underwent at least one examination that showed head circumference below the 5th percentile, head circumference could be normal in the presence of severe ventriculomegaly (seen in three fetuses). Intracranial calcifications were most commonly seen at the gray matter–white matter junction, in 15 of 17 (88%) and 28 of 28 (100%) confirmed and presumed infections, respectively. The basal ganglia and/or thalamus were also commonly involved with calcifications in 11 of 17 (65%) and 18 of 28 (64%) infections, respectively. The skull frequently had a collapsed appearance with overlapping sutures and redundant skin folds and, occasionally, intracranial herniation of orbital fat and clot in the confluence of sinuses.

Conclusion: The spectrum of findings associated with congenital Zika virus infection in the IPESQ in northeastern Brazil is illustrated to aid the radiologist in identifying Zika virus infection at imaging.

Online supplemental material is available for this article.

[1] From the Dept of Diagnostic Imaging, Federal Univ of São Paulo, São Paulo, Brazil (P.S.d.O.S., R.X., J.S.); Foundation Inst for Education and Research in Diagnostic Imaging, Dept of Diagnostic Imaging, Federal Univ of São Paulo, São Paulo, Brazil (P.S.d.O.S., J.S.); Dept of Radiology, Beth Israel Deaconess Medical Ctr, Harvard Medical School, Boston, Mass (D.L.); Instituto de Pesquisa Professor Amorim Neto, Campina Grande, PB, Brazil (A.S.d.O.M., M.M.R.A.); Instituto de Saúde Elpidio de Almeida, Campina Grande, PB, Brazil (A.S.d.O.M., M.M.R.A.); Faculdade de Ciências Médicas de Campina Grande, Campina Grande, PB, Brazil (A.S.d.O.M.); Hosp Municipal Pedro I, Serviço Municipal de Atendimento Transdisciplinar a Gestantes e Bebês com Infecção Congênita por Zika Virus, Campina Grande, PB, Brazil (A.S.d.O.M., A.G.M.B.); Universidade Federal de Campina Grande, PB, Brazil (M.M.R.A.); Laboratory of Neuropathology, State Inst of Brain, Rio de Janeiro, Brazil (L.C.); Departamento de Genética, Instituto de Biologia, Universidade Federal do Rio de Janeiro, Rio de Janeiro, Brazil (A.T., R.S.A.); Div of Ultrasound in Obstetrics & Gynecology, Lis Maternity Hosp, Tel Aviv Sourasky Medical Ctr, Sackler Faculty of Medicine, Tel Aviv Univ, Tel Aviv, Israel (G.M.); Fetal Medicine Foundation Latinamerica–FMFLA, Centrus–Fetal Medicine, Campinas, Brazil (R.X.); Boston Children's Hosp, Boston, Mass (R.R.); Inst of Biomedical Sciences and National Ctr for Structural Biology and Bioimaging, Federal Univ of Rio de Janeiro, Rio de Janeiro, Brazil (F.T.M.); and D'Or Inst for Research and Education, Rua Diniz Cordeiro 30, Botafogo, Rio de Janeiro, RJ, Brazil 22881-100 (F.T.M.). Received July 7, 2016; revision requested July 14; revision received July 22; accepted July 27; final version accepted August 3. **Address correspondence to** F.T.M. (e-mail: *Fernanda.tovarmoll@idor.org*).

Much has been written recently regarding Zika virus in pregnancy and the increased risk of microcephaly in fetuses exposed to the virus. The outbreak of infection in Brazil, especially in the northeast part of the country (1), has been of particular concern. The virus has been found in the fluids of pregnant mothers and during autopsy in the brains of neonates with microcephaly (2–5). Much of the concern in the media regarding the teratogenicity of Zika virus infection has focused on brain findings of microcephaly. However, as documented in many case series, there are a variety of brain abnormalities that can be found in fetuses exposed to intrauterine Zika virus infection (2–11). These include abnormalities in ventricular size, gray and white matter volume loss, brainstem abnormalities, and calcifications.

Although the current outbreak has centered in Brazil, according to the U.S. Centers for Disease Control and Prevention, there are currently 51 countries or territories in which active transmission of Zika virus has been reported (12). It is important for radiologists to understand the type of abnormalities associated with congenital Zika virus infection to aid in recognition of disease and appropriate counseling of patients. The purpose of this special report is to document the imaging findings associated with congenital Zika virus infection as found in patients seen at the Instituto de Pesquisa in Campina Grande State Paraiba (IPESQ) in northeastern Brazil.

Materials and Methods

This retrospective review includes imaging and autopsy data from an institutional review board–approved study that allowed for imaging and follow-up of presumed Zika virus infection in pregnant women and their neonates. Written informed consent was obtained from the pregnant women and/or the parents of newborns. From June 2015 to May 2016, 438 patients were referred to the IPESQ for one or more of the following: *(a)* pregnancy with rash, *(b)* fetal central nervous system (CNS) abnormalities at prenatal ultrasonography (US), and/or *(c)* postnatal microcephaly or other CNS malformation that was believed to be characteristic of congenital infection. During this period, 384 pregnant women with a rash or a history of CNS abnormality at US (group 1) and 47 neonates with postnatal physical examination findings suggestive of microcephaly (head circumference < 33 cm) (group 2) were enrolled in this protocol. Group 1 exclusion criteria included not returning for imaging at IPESQ, no CNS abnormality identified at US examination at IPESQ, classic findings of isolated CNS abnormality not characteristic of infection, diagnosis of a genetic syndrome or aneuploidy, and lack of postnatal images for review. Group 2 exclusion criteria included not returning for computed tomography (CT) or magnetic resonance (MR) imaging examination at IPESQ and no calcification on postnatal images. Initially, we used a head circumference criterion of 32.5 cm for microcephaly as an exclusion criterion for the postnatal diagnosis, but after review of the imaging findings, there was a newborn with normal head circumference but severe ventriculomegaly and calcifications similar to those seen in the other confirmed and presumed Zika virus infections; therefore, this neonate was included in our population with presumed Zika virus infection. After exclusions, there were imaging studies of 31 fetuses in 30 pregnant women (which included one set of twins) and 45 neonates (which included the 31 fetuses that underwent prenatal imaging, as well as an additional 14 neonates that were enrolled postnatally; Fig 1).

Results in 10 of these patients have been reported previously (4,5); however, these prior publications were not of sufficiently large sample size to provide estimates of the types of abnormalities seen in infected neonates, and the images were not formally reviewed by multiple fetal and neonatal imaging experts.

Prenatal and/or postnatal Zika virus infection investigations were performed on the patients' fluids (blood, urine, amniotic fluid, and/or cord blood) or tissues (placenta or brain and other organ tissue at autopsy), as described previously (4). In the group with confirmed infection, viral infection was confirmed by means of serologic findings or reverse transcription polymerase chain reaction (RT-PCR). An assay (Rapid Test DPP Zika IgM/IgG Assay; Chembio, Medford, NY) was used to detect immunoglobulin G and immunoglobulin M against Zika virus in the fluids. Virus genome was identified in fluids and/or tissues with RT-PCR by using specific primers and probes to identify the region of Zika virus (13). Dengue virus and chikungunya virus infection were excluded by using enzyme-linked immunosorbent assay and RT-PCR. The patients tested negative for toxoplasmosis, syphilis, varicella-zoster virus, Parvovirus B19, rubella, Cytomegalovirus, and herpes virus (TORCH) infection, as well as human immunodeficiency virus.

As described previously (4,5), prenatal US was performed by fetal medicine specialists using either a Voluson E8 unit (General Electric, Milwaukee, Wis) with transvaginal probes or a Samsung XG or WS80 unit (Samsung, Seoul, South Korea) with 2–9-MHz probes. MR imaging of the fetus was performed with a 3-T Skyra unit

Published online before print
10.1148/radiol.2016161584 **Content codes:** CT MR PD

Radiology 2016; 281:203–218

Abbreviations:
CNS = central nervous system
IPESQ = Instituto de Pesquisa in Campina Grande State Paraiba
RT-PCR = reverse transcription polymerase chain reaction
TORCH = toxoplasmosis, syphilis, varicella-zoster virus, parvovirus B19, rubella, cytomegalovirus, and herpes virus

Author contributions:
Guarantors of integrity of entire study, P.S.d.O.S., D.L., A.S.d.O.M., A.G.M.B., A.T., R.X., F.T.M.; study concepts/study design or data acquisition or data analysis/interpretation, all authors; manuscript drafting or manuscript revision for important intellectual content, all authors; approval of final version of submitted manuscript, all authors; agrees to ensure any questions related to the work are appropriately resolved, all authors; literature research, P.S.d.O.S., D.L., A.S.d.O.M., M.M.R.A., L.C., R.S.A., R.X., R.R., F.T.M.; clinical studies, P.S.d.O.S., A.S.d.O.M., A.G.M.B., L.C., G.M., R.X., R.R., F.T.M.; experimental studies, A.T., R.S.A., F.T.M.; statistical analysis, P.S.d.O.S., D.L., J.S., F.T.M.; and manuscript editing, P.S.d.O.S., D.L., A.S.d.O.M., L.C., R.S.A., G.M., R.X., R.R., J.S., F.T.M.

Conflicts of interest are listed at the end of this article.

Figure 1

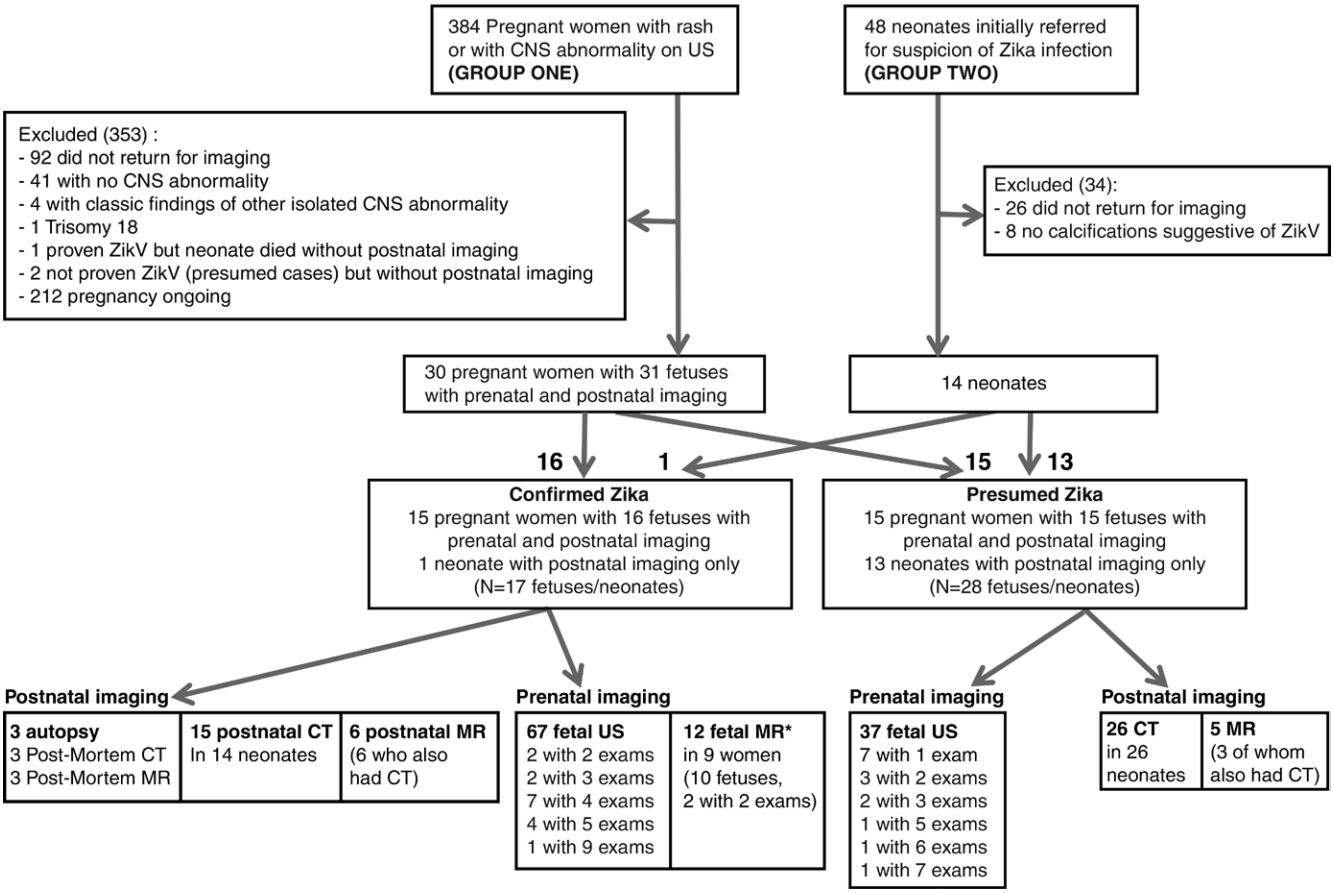

Figure 1: Flowchart for subject inclusion and exclusion in the confirmed and presumed Zika virus *(ZikV)* infection cohorts. * = Gestational ages for fetal MR examinations were 26 weeks (with a second MR examination at 30 weeks), 29 weeks, 29 weeks (with a second MR examination at 37 weeks), 32 weeks, 34 weeks, and four examinations at 36 weeks (one in a set of twins).

(Siemens Healthcare, Erlangen, Germany) or a 1.5-T Espree unit (Siemens Healthcare) with an eight-channel body coil and standard acquisition protocols (Table E1 [online]). Postnatal head CT was performed with a 16-section CT scanner (Siemens Healthcare). Postnatal MR imaging was performed with a 1.5-T Espree brain MR imaging unit (Siemens Healthcare). Postmortem brain examination was performed in stillborns or neonates who died within 48 hours of birth after obtaining parental consent to perform autopsy. Brain tissue images were acquired with a 64-channel multisection CT scanner (GE Healthcare) and a 3-T MR imaging unit (Achieva; Philips, Best, the Netherlands).

Neurological findings on prenatal MR images and postnatal CT and MR images were subjectively described by four radiologists with experience in fetal and/or neonatal neuroradiology (D.L., an obstetric and fetal MR imager with 20 years of experience; R.R. and F.T.M., pediatric neuroradiologists with 20 and 16 years of experience, respectively; and P.S.d.O.S., a neuroradiologist with 12 years of experience). Findings were agreed on in consensus. In a minority of cases, select images from obstetric US were also available for review.

Results

In the 16 women with confirmed infection (including one set of twins, yielding 17 fetuses and/or neonates), testing for Zika virus by means of RT-PCR and/or serologic analysis generated positive results in amniotic fluid in nine women (with 10 gestational sacs), cord blood in seven women, neonatal brain during autopsy in three neonates, and placenta in one neonate, with multiple positive sites in two women (one of whom had twins; Table E2 [online]). A rash characteristic of Zika virus infection was present in the first trimester in 13 of 16 women (81%) with confirmed infection (one with twins) and in 22 of 28 women (78%) with presumed infection.

The imaging findings are described in Table 1. Figures depicting fetal

Table 1

Imaging Findings in 17 Confirmed and 28 Presumed Zika Virus Infections

Abnormality	No. of Confirmed Infections at Prenatal and/or Postnatal Imaging	No. of Presumed Infections with Microcephaly and Calcifications on CT Images or Postnatal MR Images	Comments
Parenchymal volume loss	17 (100)	28 (100)	…
Mild to moderate	6 (35)	17 (61)	…
Severe	12 (70)	11 (39)	…
Cortical abnormalities	16 (94)	28 (100)	Fifteen subjects were categorized as having both polymicrogyria and irregular areas of sulci and/or gyri not otherwise specified.
Lissencephaly	2 (12)	6 (21)	…
Polymicrogyria or pachygyria	11 (65)	14 (50)	…
Irregular areas of sulci and/or gyri not otherwise specified	5 (29)	21 (75)	…
Corpus callosum abnormalities	16 (94)	22 (78)	CT findings of agenesis and/or dysgenesis of the corpus callosum were frequently difficult owing to relatively large fornices and some anterior corpus callosum being present, but pronounced colpocephaly without visualization of the body of the corpus callosum was used for this diagnosis at CT. At MR imaging and US, direct visualization of the corpus callosum was used for diagnosis.
Ventriculomegaly	16 (94)	27 (96)	It can be difficult to characterize ventriculomegaly as mild or moderate, since the occipital horns were often dilated out of proportion to the frontal horns owing to parieto-occipital gray and white matter loss. Asymmetrical venticulomegaly was observed in six of 17 and five of 28 of the confirmed and presumed infections, respectively.
Mild	4 (24)	5 (18)	…
Moderate	7 (41)	9 (32)	…
Severe	5 (29)	13 (46)	…
Septations in occipital horns	5 (29)	3 (11)	…
Cerebellum abnormalities	14 (82)	21 (75)	Twelve subjects had abnormalities of cerebellar hemispheres and vermis.
Hemisphere hypoplasia or maldevelopment	14 (82)	11 (39)	…
Vermis hypoplasia	10 (59)	19 (68)	…
Brainstem hypoplasia and/or atrophy	12 (70)	6 (21)	The high percentage in the confirmed infections reflects that these are predominantly prenatally diagnosed infections compared with the presumed infections, which has many neonates with only postnatal images. Prenatal imaging includes sagittal fetal MR imaging, which allows for better visualization of the brainstem compared with axial postnatal CT.
Calcifications	17 (100)	28 (100)	This was an inclusion criterion for the presumed infection cohort.
Periventricular	11 (65)	4 (14)	All instances with periventricular calcifications had the periventricular calcifications in areas of parenchymal thinning.
Cortical	4 (24)	4 (14)	At times, a layered appearance can be seen with cortical, gray, and white matter.
Gray matter–white matter junction	15 (88)	28 (100)	…
Basal ganglia and/or thalamus	11 (65)	18 (64)	…
Brainstem	3 (18)	4 (14)	…
Cerebellum	1 (6)	1 (4)	…
Soft tissues of the neck	0	1 (4)	…
Heterogeneous material, some of which could be thrombus in the region of the confluence of sinuses	9 (53)	8 (28)	At unenhanced CT, it is helpful to compare material in the confluence of the sinuses region to the basilar artery to determine if the attenuating and/or heterogeneous material is due to thrombus rather than dehydration and hemoconcentration effect.

Note.—Numbers in parentheses are percentages.

Figure 2

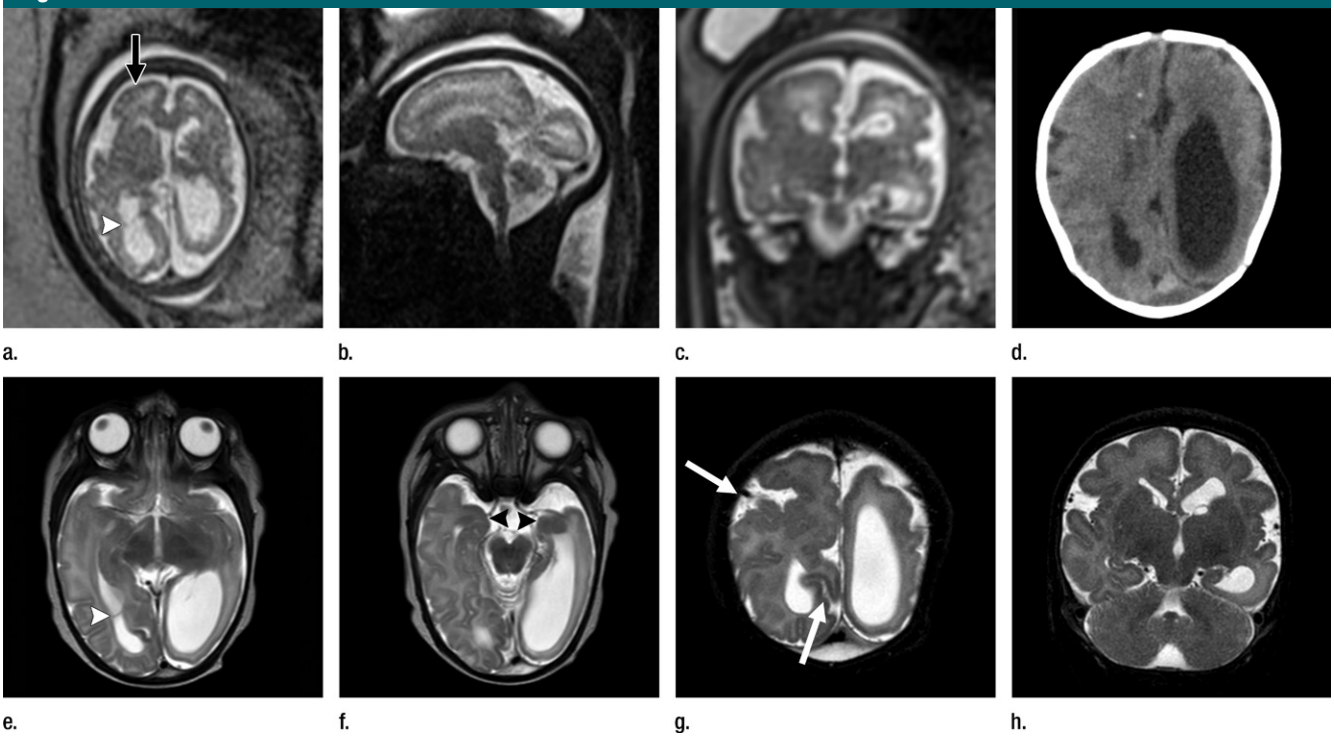

Figure 2: **(a)** Axial, **(b)** sagittal, and **(c)** coronal fetal T2-weighted MR images in a 29-year-old woman with confirmed Zika virus infection, initially seen for characteristic rash at 12 weeks of gestational age. **(d)** Axial postnatal CT image and **(e–g)** axial and **(h)** coronal T2-weighted MR images obtained in her male neonate. The fetal MR images obtained at 34 weeks (**a–c**) show asymmetrical ventriculomegaly with a septation in the right occipital horn (arrowhead on **a**), small frontal lobes, thinning of the occipital parenchyma (left worse than right), underdeveloped sylvian fissures, and regions of thickened cortex, as in the right frontal lobe, which is suggestive of polymicrogyria (arrow on **a**). There is abnormal, increased signal intensity in the white matter. The postnatal CT image (**d**) obtained in the 22-day-old neonate shows punctate calcifications at the gray matter–white matter junction and asymmetrical ventriculomegaly. The T2-weighted MR images obtained at 26 days (**e–h**) show septation in the ventricle (arrowhead on **e**). Note how the right ventricle has relatively decreased in size compared with the prenatal image, whereas the left ventricle has increased in size. Under-rotation of the hippocampus (arrowheads on **f**) is demonstrated. There is clear asymmetry of the gyral pattern on **g**, which is relatively smooth in the left occipital region, with abnormal folds in the right occipital and frontoparietal regions (arrows on **g**). Subependymal cysts are visualized on **h**, which are not seen on fetal MR images.

anatomy (Figs 2–8), neonatal microcephaly (Figs 9–15; Figs E1–E3 [online]), and one neonate with normal head circumference but with characteristic calcifications in association with severe ventriculomegaly (Fig 16) are illustrated. Movie clips of sequences of images are also available in Movies 1–E5 (online).

In all but one fetus with confirmed Zika virus infection at prenatal imaging, the head circumference percentile was at or below the 5th percentile in at least one US examination performed during the second trimester of pregnancy (Table 2). However, one fetus with severe parenchymal and brainstem malformation had severe ventriculomegaly and normal head circumference at a scan conducted at 17 weeks of gestational age, and the circumference remained within the normal range later in pregnancy. In 23 of 26 fetuses that underwent serial prenatal US, head circumference remained under the 5th percentile until birth, which led to a diagnosis of microcephaly at birth. However, it is notable that the three fetuses with head circumference in the normal range at birth showed severe ventriculomegaly, which we presume was due to the enlarged, obstructed ventricles. For this reason, we included Figure 16, which depicts a neonate referred to IPESQ for potential Zika virus infection, but the head circumference was 38 cm at birth. The CT images showed calcifications in the subcortical region, thalamus, basal ganglia, and brainstem. No sulci were seen; however, the parenchyma was extremely thin. There was pontocerebellar hypoplasia and Dandy-Walker spectrum anomaly, and the corpus callosum was not visualized.

The most remarkable change in the brain parenchyma, present on all neonatal images, was the reduction in parenchymal volume. Abnormalities of cortical development associated with volume changes were observed in 16 of 17 confirmed infections (94%) and 28 of 28 presumed infections (100%). Abnormalities of the corpus callosum were present in

Figure 3

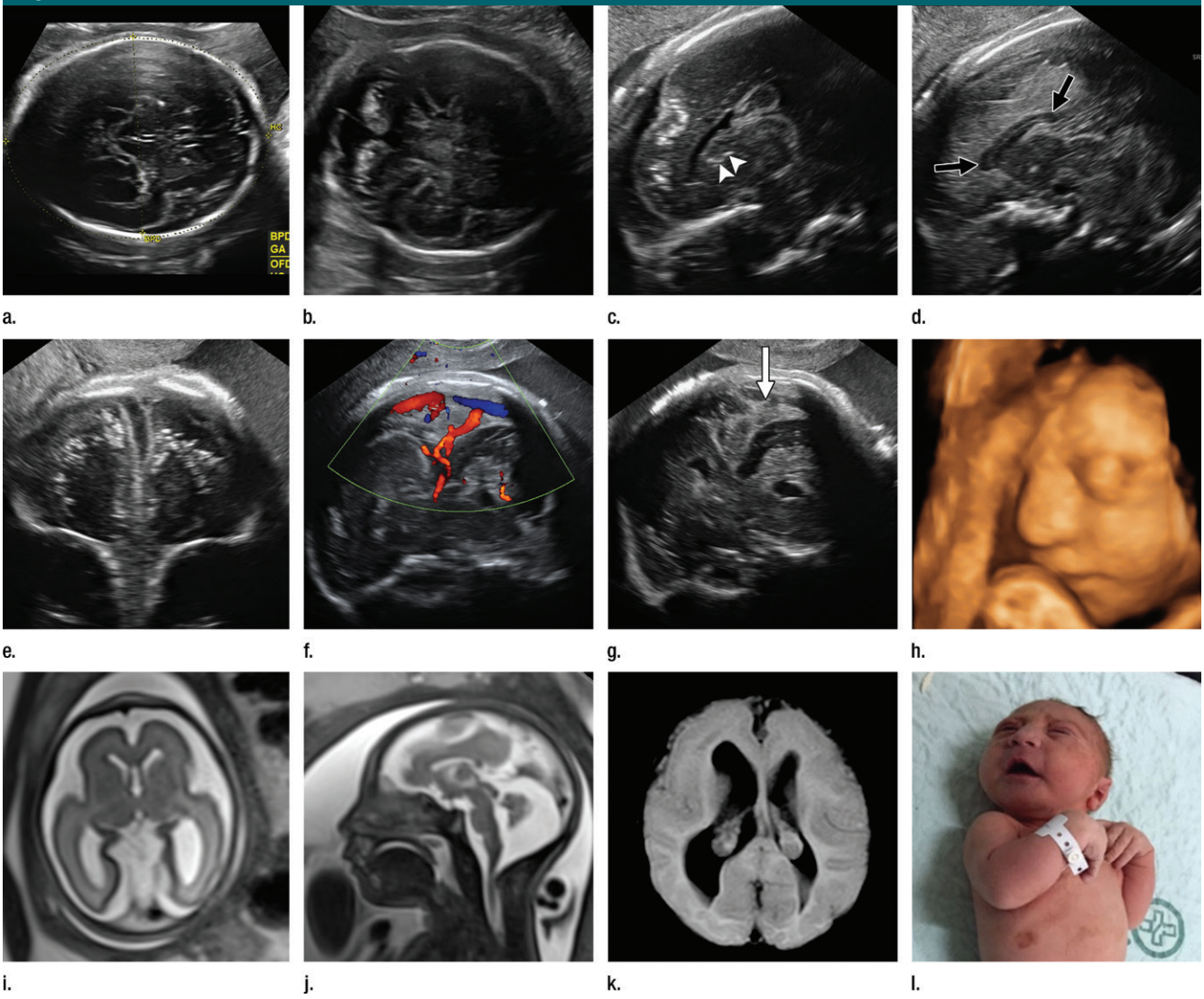

Figure 3: Images in the case of a 34-year-old woman with confirmed Zika virus infection, initially seen for a rash at 8 weeks of gestation. Fetal head circumference was in the normal range at 12 and 16 weeks (5.8 cm and 11.9 cm, respectively) but then decreased to the 10th percentile at 22 weeks and was below the 3rd percentile in subsequent imaging examinations. **(a–h)** US images obtained at 30 weeks. Head circumference on the axial image (**a**) measured 24 cm (<2.3 percentile, corresponding to a gestational age of 26 weeks 3 days). Note the open sylvian fissures and relatively smooth cortex, which are abnormal findings at this gestational age. Oblique axial image (**b**) shows cerebellar calcifications (seen as the echogenic outer contour of the cerebellar hemispheres) and inferior vermian hypoplasia with associated enlarged cisterna magna. A sagittal transvaginal image (**c**) shows calcifications in the basal ganglia (arrowheads) and more bulky calcification at the gray matter–white matter junction. Another sagittal transvaginal image (**d**) shows a relatively small corpus callosum (arrows). A coronal image (**e**) shows cortical and subcortical white matter calcifications in a linear pattern. The gyral pattern is abnormal, which is suggestive of polymicrogyria. A sagittal color Doppler image (**f**) shows a stretched appearance of vessels coursing into the posterior fossa. An oblique axial gray-scale transvaginal image in the posterior fossa (**g**) shows heterogeneous material in the confluence of sinuses due to blood clot (arrow). A three-dimensional US image of the face (**h**) shows a sloping forehead, compatible with frontal lobe hypoplasia. **(i)** Axial and **(j)** sagittal fetal MR images obtained at 29 weeks show atrophic frontal lobes, wide sylvian fissures, enlarged posterior fossa, abnormal gyral pattern, prominent cerebrospinal fluid spaces, and inferior vermian hypoplasia. On **i,** note the diffuse hypointense and undersulcated cortex, which is suggestive of mineralization and polymicrogyria. The hypoplastic corpus callosum can be seen on the sagittal view (**j**), as well as the inferior vermian hypoplasia, enlarged cisterna magna, and heterogeneous signal intensity in the confluence of sinuses. There is a subjectively thin spinal cord. **(k)** Postnatal axial MR image obtained at 81 days shows small frontal lobes and cortical thickening. The choroid plexi are enlarged. **(l)** Photograph of the neonate after birth.

Figure 4

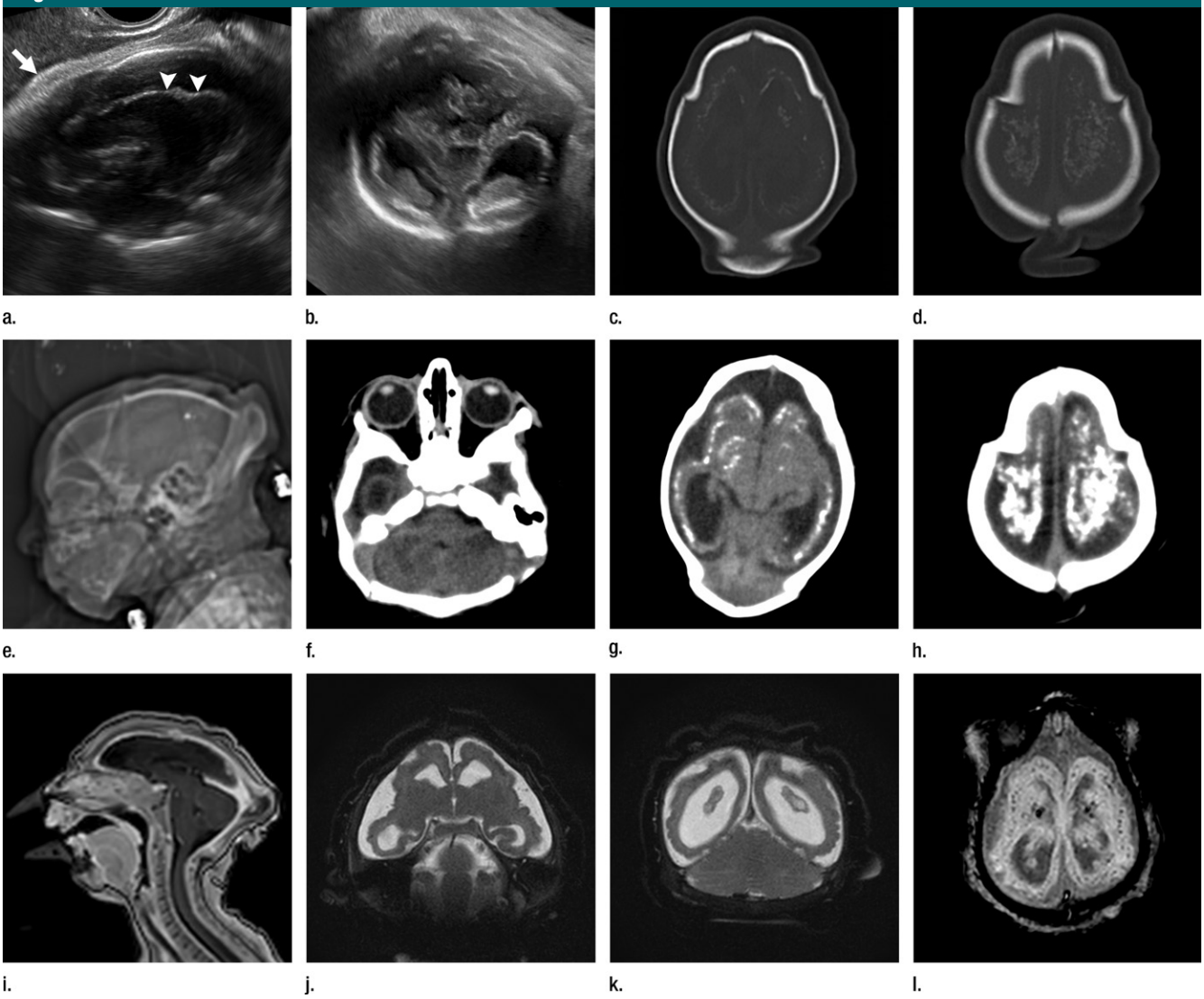

Figure 4: Images in the case of an 18-year-old woman, first seen for rash at 10 weeks of pregnancy, with confirmed Zika virus infection. US findings obtained at 20 weeks of gestational age were reportedly normal, with normal head circumference of 17.5 cm. At 37 weeks of gestational age, **(a)** sagittal transvaginal and **(b)** coronal transabdominal US images obtained with the head upside down show a small head circumference (26.4 cm, corresponding to 28 weeks 5 days, below the 3rd percentile), moderate ventriculomegaly with dense intracranial calcifications (arrowheads on **a**), and abnormal head shape with flattened appearance and thickened skin (arrow on **a**). On the sonogram, it is difficult to precisely localize the calcifications, given the thin parenchyma. **(c, d)** Axial bone window CT images, **(e)** sagittal localizer CT image, and **(f–h)** axial CT images show microcephaly with cerebral atrophy, and, despite ventriculomegaly, the extra-axial cerebrospinal fluid spaces are still prominent. The dense calcifications are predominantly located in the subcortical white matter at the gray matter–white matter interface. There is markedly abnormal skull shape with some eversion of the bones at the suture sites (particularly frontoparietal sites), with redundant skin folds (particularly in the parieto-occipital region). **(i)** Sagittal T1-weighted, **(j, k)** coronal T2-weighted, and **(l)** axial susceptibility-weighted MR images obtained at 1 month of age show an undersegmented midbrain, severe microcephaly, open sylvian fissures, and polymicrogyria. The dense calcifications are evident on the susceptibility-weighted image. On the sagittal images (**a, e, i**), note the small supratentorial compartment and associated skull deformity.

16 of 17 confirmed infections (94%) and 22 of 28 presumed infections (78%).

Lateral ventricles were enlarged in 16 of 17 confirmed infections (94%) and 27 of 28 presumed infections (96%). This was asymmetrical in six of 17 confirmed infections and five of 28 presumed infections. Despite ventriculomegaly, the extra-axial spaces are frequently still prominent because of cortical underdevelopment or atrophy. Other findings associated with the ventricles were septations in the ventricle (typically in the occipital horns), which were frequently difficult to distinguish

Figure 5

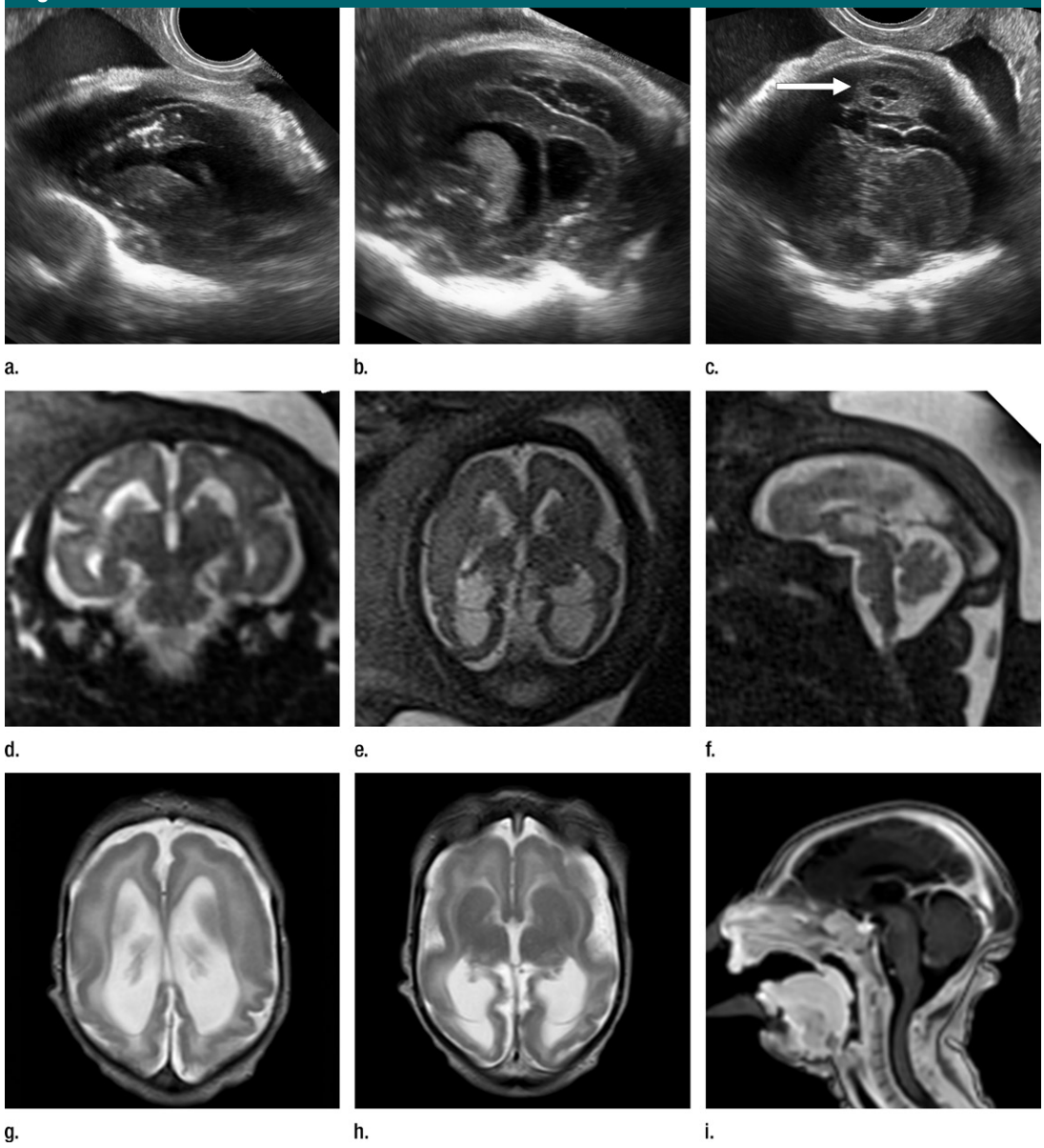

Figure 5: Images in the case of a 33-year-old woman who had a rash at 10 weeks of pregnancy, with confirmed Zika virus infection. US performed at 19 weeks of gestational age showed a head circumference in the normal range (16.6 cm). **(a, b)** Sagittal and **(c)** coronal transvaginal US images obtained at the next US examination at 27 weeks 2 days of gestational age, however, showed the fetal head circumference to be 21.6 cm, which corresponded to 23 weeks 3 days (<2.3 percentile, not shown). There was mild ventriculomegaly with septations in the occipital horns. Calcifications could be seen at the gray matter–white matter junction. The cerebrum was atrophic. There was blood clot in the region of the confluence of sinuses (arrow). **(d)** Coronal, **(e)** axial, and **(f)** sagittal T2-weighted fetal MR images obtained at 32 weeks show septations in the ventricles and an abnormal-appearing cortex, with a thickened and undersulcated cortex most marked on the left, compatible with polymicrogyria. The sagittal midline view shows microcephaly, blood clot in the region of the confluence of sinuses, and prominent skin folds. **(g, h)** Axial T2-weighted and **(i)** sagittal T1-weighted postnatal MR images obtained in the 4-week-old neonate show diffuse gyral abnormality and abnormal myelination. The septations in the ventricles are again seen. The sagittal image shows thinning of the spinal cord at the craniocervical junction.

Figure 6

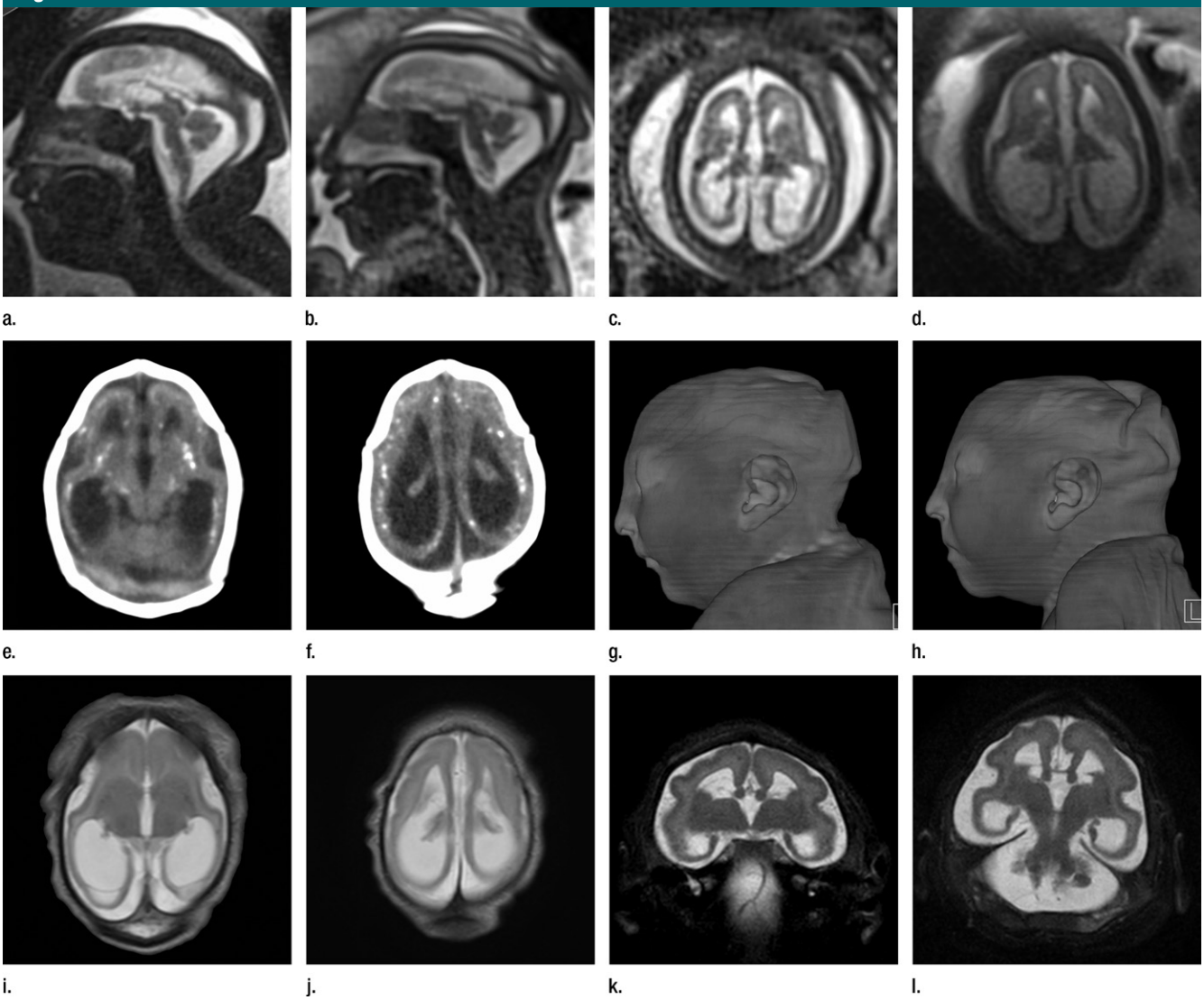

Figure 6: Images in the case of a 24-year-old woman pregnant with twins, with characteristic rash at 9 weeks of pregnancy and confirmed Zika virus infection. (For each pair of images, the first image is of twin A, and the second image is of twin B.) At 14 weeks of gestational age, the fetal head size of both twins was normal. The head size never went below the 3rd percentile for either fetus in examinations at 19–28 weeks. **(a, b)** Sagittal and **(c, d)** axial fetal MR images were obtained at 36 weeks. **(e, f)** Axial and **(g, h)** surface reconstruction postnatal CT images and **(i, j)** axial T2-weighted and **(k, l)** coronal MR images were obtained 1 week after delivery at 38 weeks of gestational age. There is severe microcephaly with profound frontal lobe hypoplasia. Calcifications in the subcortical white matter at the gray matter–white matter junction are visualized. Both twins have a flattened appearance of the pons. The spinal cord is atrophic (best seen on **a**). Redundant skin is seen in the occipital region. There is polymicrogyria involving the frontal and parietal regions and atrophic cortex and white matter in the occipital regions. Each twin has hypoplasia of the corpus callosum, with prominent fornices. There is abnormal myelination in the occipital region that, in twin A (**i**), has the appearance of a cyst or septation within the ventricle. The cerebellum is somewhat small and nodular. There is lack of rotation of the hippocampi.

from subventricular cysts. Subependymal cysts were occasionally visualized.

Abnormalities of cortical development were present in all patients but with a substantial variation regarding the type of abnormality, hemispheric symmetry, and severity (Table 1). The most common finding was irregular areas of sulci and/or gyri not otherwise specified, but focal cortical malformation was also observed. In addition, six patients had the appearance of lissencephaly. In three fetuses, this was diagnosed prenatally. Of the other three, two did not have a fetal sonogram for review, and one only underwent a scan at 10 weeks of gestation, which is too early to assign this diagnosis. The cortical development abnormalities were usually asymmetrical. In general, the sulci were less

Figure 7

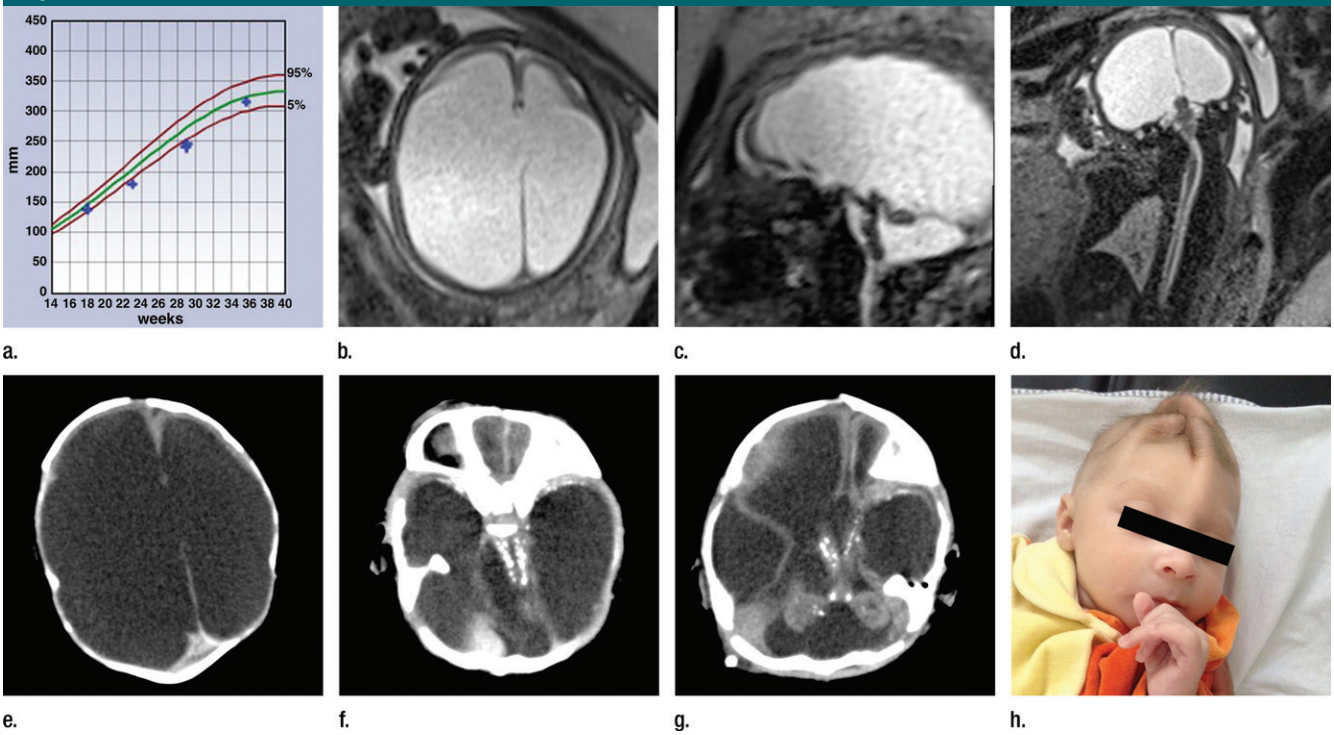

Figure 7: Images in the case of a pregnant 20-year-old woman, without history of rash, who was referred for fetal brain abnormality at US with confirmed Zika virus infection. **(a)** Graph of head circumference during pregnancy shows small head size in the second trimester, which increased in the third trimester. US (not shown) showed moderate ventriculomegaly starting at 23 weeks, which progressed to severe ventriculomegaly by the third trimester, associated with the increase in head circumference. **(b)** Axial, **(c)** sagittal, and **(d)** coronal fetal MR images obtained at 36 weeks show severe asymmetric ventriculomegaly, marked parenchymal thinning and/or atrophy, sloping forehead, and elevation of the hypoplastic cerebellar vermis with hypoplastic cerebellar hemispheres. The brainstem is thin, and the midbrain is foreshortened. The spinal cord is irregular, thin, and nonvisualized in parts, and then thicker and possibly mineralized. **(e, f)** Axial CT images obtained 1 day postnatally show severe asymmetrical ventriculomegaly with dense calcifications in the brainstem, cerebellum, and gray matter–white matter interface (temporal lobes on **f**) and marked parenchymal atrophy. **(g)** Axial CT image obtained in the 6-week-old infant, after shunting, showed persistent ventriculomegaly and periventricular, midbrain, thalamic, and cerebellar calcifications. **(h)** Photograph of the neonatal face shows redundant skin folds and skull asymmetry.

prominent, and wide sylvian and interhemispheric fissures were identified in most neonates, as well as abnormal myelination.

Calcification regions were predominantly located in the gray matter–white matter junction in our series (88% in the confirmed infection cohort and 100% in the presumed infection cohort). Calcifications were also identified in the thalamus, basal ganglia, cortex, and periventricular regions. It is important to mention that the latter were only present in neonates where there was substantial thinning of the brain parenchyma; thus, the precise location of calcifications was difficult to determine. Although less common, infratentorial calcifications were also identified. However, these were usually present in more severe manifestations of infection, being associated with dysmorphic brainstem, stenosis of the aqueduct, and secondary supratentorial hydrocephaly. Calcification in the brainstem was a common finding at autopsy (in three of three of the neonates with confirmed infection that underwent autopsy).

Abnormalities of the brainstem were identified. The pons was often thin and atrophic. There was frequently a kink seen at the pontomedullary junction. The spinal cord was thinned and at times irregular in its appearance. Other posterior fossa abnormalities included cerebellar hemisphere hypoplasia, vermis hypoplasia, and elevation of the vermis, associated with an enlarged cisterna magna.

Abnormalities of the corpus callosum—usually thin, dysgenetic, and hypoplastic or even absent—were frequently observed. Other changes included under-rotation of the hippocampus and thickened fornices.

In some imaging studies, an enlarged confluence of the dural venous sinuses had heterogeneous material. In a few fetal sonograms that were available for review, this was demonstrated to be blood clot (Fig 3g). In many postnatal CT studies, there was hyperattenuating material in this region, which could be either thrombus or hematocrit effect (due to dehydration with hemoconcentration). In many

Figure 8

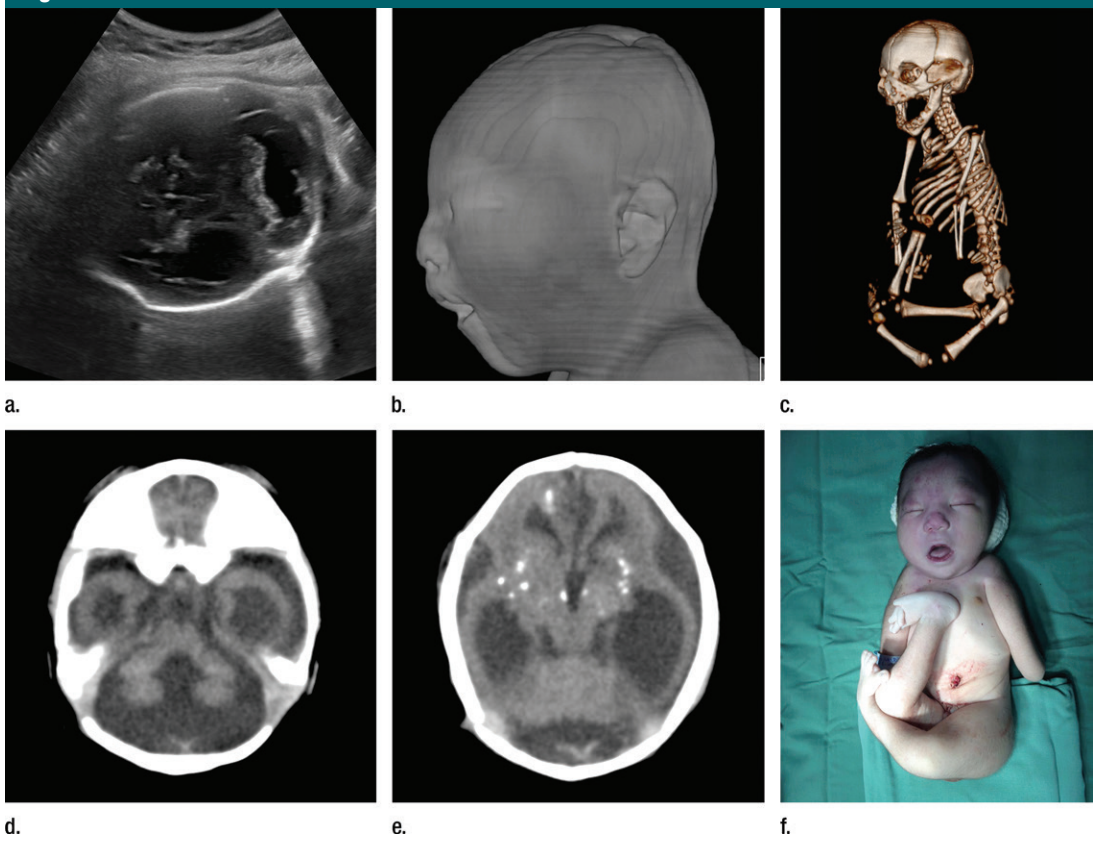

Figure 8: Fetal and postnatal images in the case of an 18-year-old pregnant woman initially seen for a rash at 12 weeks of gestation, with confirmed Zika virus infection. Signs of joint contractures were identified at US at 17 weeks, but head circumference was in the normal range, then decreased to the 15th percentile at 21 weeks and was below the 3rd percentile at subsequent scans at 24 and 36 weeks (19.0 cm and 25.0 cm, respectively). **(a)** Axial transabdominal US performed at 36 weeks shows ventriculomegaly, calcifications in the thalamus and basal ganglia, and enlarged cisterna magna. **(b)** Soft-tissue, **(c)** body bone reconstruction, and **(d, e)** axial postmortem CT images show an abnormal profile, moderate ventriculomegaly, parenchymal atrophy, splaying of the cerebellar hemispheres, inferior vermian hypoplasia, and calcifications in the subcortical white matter, thalamus, and basal ganglia. The corpus callosum is not visualized. The gyral pattern is abnormally smooth for a term neonate. The postnatal bone reconstruction image showed the severe joint contractures, similar to those observed on **(f)** a photograph of the neonate.

fetal and neonatal MR studies, there was fluid posterior to the confluence of the sinuses that was either similar to cerebrospinal fluid in attenuation or signal intensity or contained fluid with a higher protein content than that of cerebrospinal fluid. The location of the fluid collection is likely related to the unusual head shape and overlapping sutures. This abnormal head shape was frequently associated with redundant skin folds.

Other findings include orbital abnormalities, such as asymmetrical microphthalmia, cataracts, and herniation of the orbital fat into the cranial vault. Body abnormalities included arthrogryposis.

Discussion

Zika virus is a single-strand RNA Flavivirus (1). It is transmitted by infected female mosquito vectors, such as the *Aedes aegypti* mosquito. Diagnosis of Zika virus infection is complicated by the fact that it is asymptomatic in up to 80% of infections (14). The common symptoms tend to be mild and nonspecific, including headache, fever, and rash. Other symptoms include conjunctivitis, and, in rare instances, Guillain-Barré syndrome (15).

It is well recognized that Zika virus crosses the fetal-placental barrier. Zika virus has been isolated from the brain and cerebrospinal fluid of neonates born with congenital microcephaly and identified in the amniotic fluid and placental tissue of mothers who had experienced clinical symptoms consistent with Zika virus infection during their pregnancies (2–5,8,15,16). Zika virus has also been shown to lead to neurotoxiticity and to impair human neurosphere growth in experimental models (17).

Figure 9

Figure 9: Axial CT image in a 1-week-old female neonate with a head circumference of 31 cm at birth and presumed Zika virus infection. The frontal lobes are slightly hypoplastic, with mild underopercularization of the hypoplastic sylvian fissures. There are scattered subcortical calcifications (arrowheads), and there is high-attenuating material (arrow) in the region of the confluence of sinuses, likely representing blood products.

Figure 10

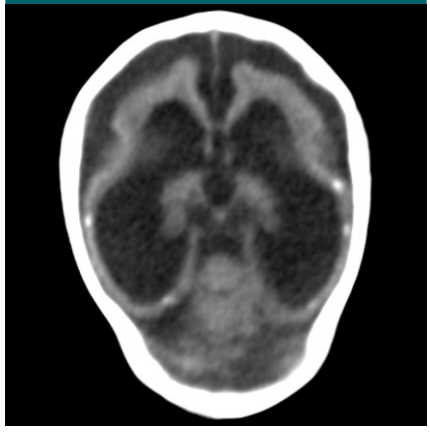

Figure 10: Oblique axial CT image in a 3-month-old male infant with a head circumference of 27.5 cm at birth, with presumed Zika virus infection. Note the misshapen skull, ventriculomegaly, absent corpus callosum, diffuse parenchymal volume loss, diffuse cortical migrational abnormality, and calcifications, most likely subcortical but difficult to classify secondary to parenchymal thinning.

Figure 11

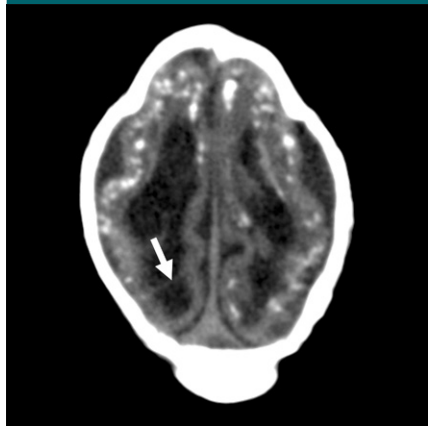

Figure 11: Axial CT image in a 1-month-old male neonate with a head circumference of 27 cm at birth, with presumed Zika virus infection. Note ventriculomegaly with septation (arrow) in the right occipital horn and striking subcortical calcifications. There are also cortical and periventricular calcifications. The gyral pattern is diffusely abnormal, and the skull is deformed.

Figure 12

Figure 12: Oblique coronal CT image in a 1-month-old male neonate with a head circumference of 29.5 cm at birth, with presumed Zika virus infection. Note the misshapen skull; ventriculomegaly; absent corpus callosum; cerebellar hypoplasia (arrows); thin parenchyma with diffuse gyral abnormality; calcifications in the thalamus, basal ganglia, and subcortical white matter; and cerebellar hemispheres.

Figure 13

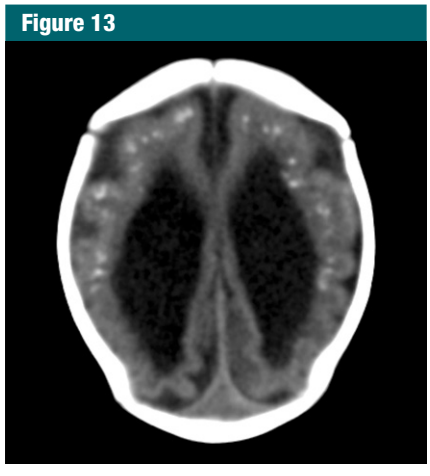

Figure 13: Axial CT image in a 1-month-old female neonate with a head circumference of 31 cm at birth, with presumed Zika virus infection. Note severe ventriculomegaly, subcortical calcifications, and diffuse gyral abnormality.

Figure 14

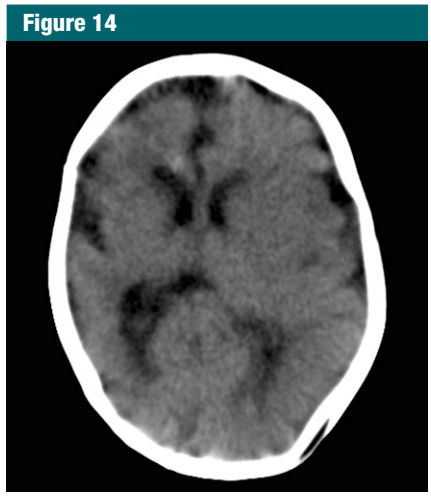

Figure 14: Axial CT image in a 2-month-old female infant with a head circumference of 32.5 cm at birth, with presumed Zika virus infection. Note the asymmetrical volume loss, more marked on the right than the left. Also note the diffusely irregular sulci and gyri bilaterally.

Microcephaly is a nonspecific term that refers to a head circumference smaller than normal for gestational age. There are many causes of microcephaly, the most common being infections (such as TORCH infections and human immunodeficiency virus), teratogens (including maternal exposure to heavy metals, alcohol, and radiation), genetic abnormalities and syndromes, and growth restriction. In the case of Zika virus, it is clear that there are developmental insults that lead to micrencephaly (small brain) and associated microcephaly (small head) (6,18–21). It is important to recognize that almost all of the infections at our institution

occurred in women who had a characteristic rash in the late first trimester. This correlates well with the finding of severe cerebral dysmorphisms associated with infection during a time of rapid brain development. According to the U.S. Centers for Disease Control and Prevention, the risk of microcephaly after maternal infection with Zika virus in the first trimester of pregnancy is 1%–13% (22). However, as the flow of women referred to the IPESQ for assessment demonstrates, it is clear that many pregnant women with a rash in Brazil are never shown to have congenitally infected fetuses, although some certainly could have less severe infection that has thus far been undiagnosed. For women who have neonates with findings suggestive of severe microcephaly but who have a history of rash or for those who had a rash in the third trimester, we can hypothesize that there was an unrecognized or asymptomatic first-trimester exposure and/or infection.

Figure 15

Figure 15: Axial CT image in a 3-month-old female infant with cord blood positive for Zika virus (confirmed Zika virus infection) and a head circumference of 28.5 cm at birth. The mother had a rash at 12 weeks. Bilateral cataracts are seen, as well as abnormal cerebellar vermis and fat herniating posteriorly from the orbits through the superior orbital fissure into the cranial vault.

As of July 2, 2016, the Brazilian Ministry of Health had been notified of 8301 cases of microcephaly and confirmed 1656 infections (23). In a recent study, França et al reported on the follow-up of 1501 cases in which Zika virus infection was suspected, of which 602 were deemed to be definitely or probably due to Zika virus (76 definite infections, 54 highly probable infections, 181 moderately probable infections, and 291 somewhat probable infections) (24). The incidence of confirmed infection in our study with respect to referral population is similar to what has been seen in the larger Brazilian population. In our study, of 432 women initially screened, only findings in 44 patients are reported here after applying our exclusion criteria. In the report by França et al, one in five definite or probable Zika virus infections yielded head circumferences in the normal range (more than −2 standard deviations below the median of the International Fetal and Newborn Growth Consortium for the 21st Century, or INTERGROWTH-21st, standard), and for one-third of definite and probable infections, there was no history of a rash during pregnancy (24). This suggests that our series is biased to the more severe infections. However, in the series by França et al (24), the more severe infections were localized in the northeast region of Brazil, since 97% of definite or probable infections were from the northeast region, where 28% of all births in Brazil occur. This suggests that there could be additional unknown factors that exacerbate the fetal infection in this region. Coinfections, in addition to those already excluded, as well other environmental factors, will need to be explored further.

There are many nomograms for head circumference size. Current guidance in Brazil is to use the standards from the INTERGROWTH-21st study for fetuses (25), the INTERGROWTH-21st study for infants (25), and World Health Organization criteria for full-term neonates (26). These charts show that a head circumference of 32 cm is at about −2

Figure 16

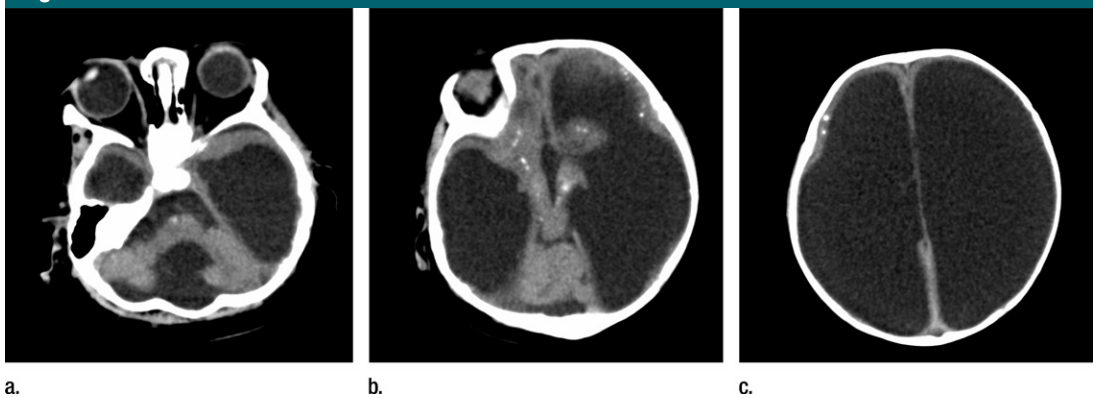

a. b. c.

Figure 16: Axial CT images in a 5-month-old male infant with a head circumference of 38 cm at birth. The mother had a rash at 11 weeks. The size of the head is likely secondary to hydrocephalus. Unlike most of our cohort, the head was still round in shape. However, calcifications are present in the subcortical region, thalamus, basal ganglia, and brainstem. No sulci were seen; however, the parenchyma is extremely thin. There is pontocerebellar hypoplasia, nonvisualization of the corpus callosum, and Dandy-Walker spectrum anomaly. This is an example of how Zika virus infection can be missed if only newborns with microcephaly are assessed.

Table 2

Head Circumference Percentiles with Respect to Gestational Age in Fetuses with Prenatal US Images

Infection Group and Case No.	Gestational Age						Head Circumference at Birth (cm)	Gestational Age at Birth (wk)
	14–16 Weeks	17–20 Weeks	21–24 Weeks	25–30 Weeks	31–35 Weeks	≥36 Weeks		
Confirmed infection								
C1	…	5	…	<3	5	40	36.5	41
C2	5	5	5	3–5	<3	3	30.5	40
C3	…	50	90	25	…	…	35	36
C4	…	…	25	…	3	<3	31.5	41
C5	50	25	…	5	5	<5	33	39
C6	…	10	5	5	…	25	35	39
C7	…	50	…	<3	<3	<3	28	39
C8	…	50	…	5	<3	…	28.5	39
C9	25	25	…	3–5	…	…	28	38
C10	5	5	…	3	…	…	26	38
C11	…	…	50	5	3	<3	29	40
C12	25	5	10	…	…	<3	29.5	40
C13	…	50	…	…	…	<3	28	40
C14	…	…	…	…	25	3	30	41
C15	50	…	50	…	5	…	32.5	41
C16	…	…	10	…	…	<3	27.5	39
Presumed infection								
P1	…	…	10	5	…	…	31	38
P2	10	50	…	5	<3	…	27	38
P3	…	…	…	…	<3	…	28.5	40
P4	…	10	…	…	…	…	29	40
P5	…	40	50	<3	3	3	31	39
P6	…	…	…	…	…	<3	27.5	39
P7	…	25	5	…	<3	…	31	39
P8	…	…	…	5	…	<1	30	39
P9	…	…	5	…	<3	…	28	39
P10	…	75	25	25	3	3	31.5	40
P11	…	…	…	…	<3	…	27	36
P12	50	25	…	…	…	…	27	38
P13	…	…	25	…	…	<1	30	37
P14	…	…	…	…	…	<3	29	39
P15	…	…	…	<3	…	…	29.5	40

Note.—Data are percentages, unless indicated otherwise. If more than one examination was conducted in a given time period, measurements from the first examination were used.

standard deviations below the mean for both boys and girls at term. However, this threshold will naturally include some normally developing neonates and also be inaccurate for neonates born prematurely. However, it should be recognized that to cast a broad net to find neonates with congenital Zika virus infection, we must bear in mind that not all neonates will have microcephaly at birth.

The striking imaging features of the severe micrencephaly associated with Zika virus include a markedly abnormal head shape. The unusual appearance of the skull, we hypothesize, is due to a combination of the small brain as it develops and a result of what, at some point, was likely a larger head size (due to ventriculomegaly) that then decompresses. Cerebral atrophy may also contribute, giving the skull the collapsed shape with everted and/or cupped sutures and overriding bones in the occipital region, causing redundant and folded skin. In part, this is also likely due to the head and skin continuing to grow, while the size of the brain regresses. However, in some fetuses and/or neonates, the ventricle and/or brain atrophy has not yet occurred, and in these instances, a normal (or even increased) head circumference may be present.

Another unusual finding that suggests skull collapse is that neonates have orbital fat herniation into the cranial vault. Thus, some of the ocular findings could be secondary to the process of skull deformation itself rather than direct infection of the eye. For example, nerve and blood flow interruption could be due to herniated tissue.

We used brain calcifications as inclusion criteria for the postnatal assessment to exclude microcephaly from causes other than infection, such as

unrecognized prematurity or congenital syndromes. While this could have led to exclusion of some infections without intracranial calcifications, it led to a homogeneous group of neonates with strikingly similar parenchymal abnormalities. In our series, the most common location for calcifications was the gray matter–white matter junction (88% in the confirmed infection cohort and 100% in the presumed infection cohort), which is an area not classically or commonly targeted in other congenital infections. The location of the calcifications at the gray matter–white matter interface could suggest a vascular component to the infection, as other processes that preferentially affect the gray matter–white matter junction have been posited to be due to changes in arterial configuration from straight vessels in the cortex to coiled vessels in the subcortical white matter (27).

In the classic TORCH infections, the brain calcifications are periventricular and cortical, although rare cases of basal ganglia and thalamus calcifications have been reported (28,29). Other findings include intraventricular adhesions, callosal abnormalities, periventricular pseudocysts, sulcation, and gyral abnormalities (29–31), similar to what we describe in this report.

However, unlike most patients with congenital Cytomegalovirus, the patients with documented or presumed Zika virus infection described in this report had severe microcephaly. This may be due to the first-trimester nature of most of the infections reported herein. It could also be due to the viral load in the Zika virus infections, which we assume are severe infections. It could be that congenital Cytomegalovirus is diagnosed in a range of infections from mild to severe, whereas we may be focusing our results on the severe Zika virus infections. In our cohort, almost all fetuses and neonates had dramatically abnormal cerebral volume, abnormal cortical folding pattern, and/or regions of lissencephaly, pachygyria, and/or polymicrogyria. We hypothesize that the cortical abnormalities visualized are due at least in part to arrested cortical development at various stages.

There have been many reports of small series of imaging findings in fetuses and neonates with congenital Zika virus infection. In 2016, Mlakar et al described one pregnancy at 29 weeks with microcephaly and intracranial calcifications, with an earlier, second-trimester sonogram that showed no abnormality (6). Also in 2016, Calvet et al described two pregnant women who underwent US at 22 weeks, which showed microcephaly (2). Sarno et al described a stillbirth at 32 weeks, with microcephaly, intracranial calcifications, and fetal hydrops (7). Driggers et al in 2016 described decreased fetal head circumference between 16 and 21 weeks, with brain abnormalities (8). In a study by Brasil et al (3), of 88 pregnant women with rash, 72 tested positive for Zika virus. Fetal US was performed in 42 fetuses, and abnormalities were seen in 12, including intrauterine growth restriction with or without microcephaly and ventricular calcifications (3).

Schuler-Faccini et al described 35 neonates with microcephaly, including brain calcifications, ventriculomgaly, and cortical and/or subcortical atrophy (9). In 2016, Hazin et al (10) and de Fatima Vasco Aragao et al (11) each described 23 neonates with microcephaly who had CT findings that included intracranial calcifications, ventriculomegaly, abnormal gryal pattern, and abnormal white matter attenuation. Guillemette-Artur et al described three neonates with congenital Zika virus infection, with micrencephaly in all three, small cerebellum in two, occipital subependymal pseudocysts in two, polymicrogyria in three, corpus callosum abnormalities in two, and hypoplastic brainstem in one (32). These findings are all similar to what we report.

Our study had limitations. What we present here is a convenience sample of imaging findings for illustrative purposes. Our cohort was obtained from a referral center for high-risk pregnancy. Thus, we have no information on incidence of the Zika virus in the general population or risk estimates for transmission to the fetus. Because of the manner in which we accrued subjects, neonates with congenital infection but with normal head size or brain abnormalities without calcifications could have been missed. In addition, it could be that some of the cohort had disease origin for microcephaly other than Zika virus. For example, we excluded a neonate with microcephaly and confirmed Zika virus infection due to aneuploidy with trisomy 13 syndrome. However, other infections or syndromes could be present but not yet identified in either our confirmed infection cohort or our presumed infection cohort. Findings on MR images can lead to underestimation of the incidence of calcifications, and evaluation of CT images makes characterization of subtle parenchymal abnormalities and corpus callosum abnormalities difficult. Further imaging studies on these neonates as they grow will be helpful in further assessment of areas involved with the infection. Finally, we focused on brain findings in this review. Additional sites of infection and associated pathologic abnormalities will likely be identified in the future.

It is well recognized that transplacental transmission of viruses, even in subclinical maternal infection, can lead to severe congenital abnormalities. As in other infections, serial imaging can demonstrate evolution of findings. Prenatal sonograms may show normal or decreased head circumference and, rarely, increased head circumference. Almost all neonates will show intraparenchymal calcifications more severe than what are typically seen in TORCH infections and frequently occur at the gray matter–white matter junction, which is an unusual location for the calcifications of other congenital infections. We hope the illustrations of these many fetuses and neonates will aid others in the event that the unfortunate epidemic of congenital Zika virus continues.

Acknowledgments: We gratefully acknowledge the members of the Brazilian Network BRAZIKA (Rede Internacional de Estudos Sobre Zika no Brasil).

Disclosures of Conflicts of Interest: P.S.d.O.S. disclosed no relevant relationships. **D.L.** Activities related to the present article: disclosed no relevant relationships. Activities not related to the present article: author received royalties from Elsevier and UpToDate. Other relationships: disclosed no relevant relationships.

A.S.d.O.M. disclosed no relevant relationships. **M.M.R.A.** disclosed no relevant relationships. **A.G.M.B.** disclosed no relevant relationships. **L.C.** disclosed no relevant relationships. **A.T.** disclosed no relevant relationships. **R.S.A.** disclosed no relevant relationships. **G.M.** disclosed no relevant relationships. **R.X.** disclosed no relevant relationships. **R.R.** disclosed no relevant relationships. **J.S.** disclosed no relevant relationships. **F.T.M.** disclosed no relevant relationships.

References

1. Campos GS, Bandeira AC, Sardi SI. Zika virus outbreak, Bahia, Brazil. Emerg Infect Dis 2015;21(10):1885–1886.
2. Calvet G, Aguiar RS, Melo AS, et al. Detection and sequencing of Zika virus from amniotic fluid of fetuses with microcephaly in Brazil: a case study. Lancet Infect Dis 2016;16(6):653–660.
3. Brasil P, Pereira JP Jr, Raja Gabaglia C, et al. Zika virus infection in pregnant women in Rio de Janeiro—preliminary report. N Engl J Med 2016 Mar 4. [Epub ahead of print]
4. Melo A, Aguiar R, Amorim M, et al. Congenital Zika virus infection: beyond neonatal microcephaly. JAMA Neurol (in press).
5. Oliveira Melo AS, Malinger G, Ximenes R, Szejnfeld PO, Alves Sampaio S, Bispo de Filippis AM. Zika virus intrauterine infection causes fetal brain abnormality and microcephaly: tip of the iceberg? Ultrasound Obstet Gynecol 2016;47(1):6–7.
6. Mlakar J, Korva M, Tul N, et al. Zika virus associated with microcephaly. N Engl J Med 2016;374(10):951–958.
7. Sarno M, Sacramento GA, Khouri R, et al. Zika virus infection and stillbirths: a case of hydrops fetalis, hydranencephaly and fetal demise. PLoS Negl Trop Dis 2016;10(2):e0004517.
8. Driggers RW, Ho CY, Korhonen EM, et al. Zika virus infection with prolonged maternal viremia and fetal brain abnormalities. N Engl J Med 2016;374(22):2142–2151.
9. Schuler-Faccini L, Ribeiro EM, Feitosa IM, et al. Possible association between Zika virus infection and microcephaly—Brazil, 2015. MMWR Morb Mortal Wkly Rep 2016;65(3):59–62.
10. Hazin AN, Poretti A, Turchi Martelli CM, et al. Computed tomographic findings in microcephaly associated with Zika virus. N Engl J Med 2016;374(22):2193–2195.
11. de Fatima Vasco Aragao M, van der Linden V, Brainer-Lima AM, et al. Clinical features and neuroimaging (CT and MRI) findings in presumed Zika virus related congenital infection and microcephaly: retrospective case series study. BMJ 2016;353:i1901.
12. Centers for Disease Control and Prevention. All Countries & Territories with Active Zika Virus Transmission. http://www.cdc.gov/zika/geo/active-countries.html. Updated July 26, 2016. Accessed July 29, 2016.
13. Lanciotti RS, Kosoy OL, Laven JJ, et al. Genetic and serologic properties of Zika virus associated with an epidemic, Yap State, Micronesia, 2007. Emerg Infect Dis 2008;14(8):1232–1239.
14. Duffy MR, Chen TH, Hancock WT, et al. Zika virus outbreak on Yap Island, Federated States of Micronesia. N Engl J Med 2009;360(24):2536–2543.
15. Faria NR, Azevedo RdoS, Kraemer MU, et al. Zika virus in the Americas: early epidemiological and genetic findings. Science 2016;352(6283):345–349.
16. Martines RB, Bhatnagar J, Keating MK, et al. Notes from the field: evidence of Zika virus infection in brain and placental tissues from two congenitally infected newborns and two fetal losses—Brazil, 2015. MMWR Morb Mortal Wkly Rep 2016;65(6):159–160.
17. Garcez PP, Loiola EC, Madeiro da Costa R, et al. Zika virus impairs growth in human neurospheres and brain organoids. Science 2016;352(6287):816–818.
18. Rasmussen SA, Jamieson DJ, Honein MA, Petersen LR. Zika virus and birth defects—reviewing the evidence for causality. N Engl J Med 2016;374(20):1981–1987.
19. Besnard M, Eyrolle-Guignot D, Guillemette-Artur P, et al. Congenital cerebral malformations and dysfunction in fetuses and newborns following the 2013 to 2014 Zika virus epidemic in French Polynesia. Euro Surveill 2016;21(13).
20. de Paula Freitas B, de Oliveira Dias JR, Prazeres J, et al. Ocular findings in infants with microcephaly associated with presumed Zika virus congenital infection in Salvador, Brazil. JAMA Ophthalmol 2016 Feb 9. [Epub ahead of print]
21. Miranda-Filho DdeB, Martelli CM, Ximenes RA, et al. Initial description of the presumed congenital Zika syndrome. Am J Public Health 2016;106(4):598–600.
22. Johansson MA, Mier-y-Teran-Romero L, Reefhuis J, Gilboa SM, Hills SL. Zika and the risk of microcephaly. N Engl J Med 2016;375(1):1–4.
23. Brazilian Ministry of Health. Ministério da Saúde Confirma 1.656 Casos de Microcefalia. http://portalsaude.saude.gov.br/index.php/cidadao/principal/agencia-saude/24437-ministerio-da-saude-confirma-1-656-casos-de-microcefalia. Updated July 7, 2016. Accessed July 7, 2016.
24. França GV, Schuler-Faccini L, Oliveira WK, et al. Congenital Zika virus syndrome in Brazil: a case series of the first 1501 livebirths with complete investigation. Lancet 2016 Jun 29. [Epub ahead of print]
25. Papageorghiou AT, Ohuma EO, Altman DG, et al; International Fetal and Newborn Growth Consortium for the 21st Century (INTERGROWTH-21st). International standards for fetal growth based on serial ultrasound measurements: the Fetal Growth Longitudinal Study of the INTERGROWTH-21st Project. Lancet 2014;384(9946):869–879.
26. World Health Organization. Head Circumference-for-Age. http://www.who.int/childgrowth/standards/hc_for_age/en/. Accessed June 12, 2016.
27. Nonaka H, Akima M, Hatori T, Nagayama T, Zhang Z, Ihara F. The microvasculature of the cerebral white matter: arteries of the subcortical white matter. J Neuropathol Exp Neurol 2003;62(2):154–161.
28. Estroff JA, Parad RB, Teele RL, Benacerraf BR. Echogenic vessels in the fetal thalami and basal ganglia associated with cytomegalovirus infection. J Ultrasound Med 1992;11(12):686–688.
29. Picone O, Simon I, Benachi A, Brunelle F, Sonigo P. Comparison between ultrasound and magnetic resonance imaging in assessment of fetal cytomegalovirus infection. Prenat Diagn 2008;28(8):753–758.
30. Moinuddin A, McKinstry RC, Martin KA, Neil JJ. Intracranial hemorrhage progressing to porencephaly as a result of congenitally acquired cytomegalovirus infection—an illustrative report. Prenat Diagn 2003;23(10):797–800.
31. Teissier N, Fallet-Bianco C, Delezoide AL, et al. Cytomegalovirus-induced brain malformations in fetuses. J Neuropathol Exp Neurol 2014;73(2):143–158.
32. Guillemette-Artur P, Besnard M, Eyrolle-Guignot D, Jouannic JM, Garel C. Prenatal brain MRI of fetuses with Zika virus infection. Pediatr Radiol 2016;46(7):1032–1039.